

Simulation of Muscle-Based Orofacial Movement Dynamics using a Muscle Activation Dependent Varying Constitutive Law

Mohammad A. NAZARI,
ICP/GIPSA Lab
UMR CNRS 5216
Grenoble INP
France
Mohammad.Nazari@gipsa-lab.grenoble-inp.fr

Pascal PERRIER
ICP/GIPSA Lab
UMR CNRS 5216
Grenoble INP
France
Pascal.Perrier@gipsa-lab.grenoble-inp.fr

Matthieu CHABANAS
ICP/GIPSA Lab
UMR CNRS 5216
Grenoble INP
France
Matthieu.Chabanas@gipsa-lab.grenoble-inp.fr

Yohan PAYAN
TIMC-IMAG
UMR CNRS 5525
Université Joseph Fourier
Grenoble
France
Yohan.Payan@ima.g.fr

Abstract

This paper presents a dynamic biomechanical model of the face. It is implemented with a finite element method in the ANSYS software environment. A three layered mesh adapted to the description of the complex face muscles' courses have been defined. Soft tissues are modelled using a hyperelastic law. The variations of muscle tissues' mechanical properties associated with muscle activation are functionally accounted for and their influence on facial mimics and movements are assessed, in particular in the context of speech gestures.

Keywords: biomechanics, FEM, muscle active force, hyperelastic law

1. Introduction

In the context of clinical studies of functional consequences of maxillo-facial surgery or in the context of researches about facial gestures in face-to-face human communication, a fruitful approach consists in using biomechanical models of the face that account as realistically as possible for the mechanical properties of facial tissues. Since facial tissues are in a very large part made of muscles, a realistic modelling of the mechanical properties of muscle tissues is a main challenge. The total force generated in a muscle is the sum of two components: an active (F_{ac}) one and a passive (F_{pc}) one. Due to α -motoneuron depolarization, muscle fibres generate force, which in turn causes change in length of muscle. The force generated through the actin-myosin cross-bridges is the active component of muscle force. Due to their stiffness the surrounding tissues will resist to the active component thus defining a passive component

of muscle force. This passive component is not isotropic since the mechanical properties in the direction of muscle collagen fibres are different from the embedding matrix [1]. The passive material behaviour can be modelled with a hyperelastic transversely isotropic material[2][3][4][5].

The very first model of the active part of muscle force was proposed by [6]. According to this basic model a contractile element generates force as a function of muscle length (F versus L curve) and its velocity (F versus V curve). These curves are assumed to be scaled up or down as function of level of activation [7]. More recently authors within finite element framework have modelled the muscle force by designing new elements which include both active and passive transversal isotropy [4][5]. These elements need to be oriented along the axis of isotropy [8] to define fibre and cross fibre directions and also they should be distinguished from the surrounding tissues [9]. This method has been implemented by [10] for modelling face muscles and speech behaviours quasistatically. Many other physically-based models of the human face were developed in the framework of computer graphics facial animation [11][12], computer aided surgery [13][14] or speech production study [15][16]. The pioneer work of [11] has made popular a discrete modelling framework, with sparse mass-spring entities regularly assembled inside facial tissues. This approach allows a fast computation time with a simple algorithmic implementation. However, in addition to the lack of accuracy of such models and to their numerical instabilities, it seems to be very difficult to set their elastic parameters (the stiffness of springs) in order to fit the constitutive behaviour that is observed and measured on living tissues. A precise control of the volumetric tissue stiffness through the control of elastic parameters of springs is therefore probably unreachable

Permission to make digital or hard copies of all or part of this work for personal or classroom use is granted without fee provided that copies are not made or distributed for profit or commercial advantage and that copies bear this notice and the full citation on the first page. To copy otherwise, to republish, to post on servers, or to redistribute to lists requires prior specific permission and/or a fee.
OPAL-09, June 26-27, 2009, Vancouver, BC, CA
Copyright remains with the author(s).

for such discrete models. For this reason, in the continuity of the models developed by [13] and [12], we have chosen to use the Finite Element method to model the continuous behaviour of human facial tissues. The model, originally presented by [17] in its first version, is detailed in the following section.

2. Model and Its Specification

The 3D finite element model consists of three parts and has been implemented in ANSYS (R) release 11.0 software. The main part is a mesh which models the facial tissues. Cable elements (i.e. force generators) and contact elements are other important constituents of the model.

2.1 Main face mesh: modelling the passive tissues

The main mesh is a finite element discretization of the volume defined by the facial tissues located between the skull and the external skin surface of the face. It is based on a previous continuous face model [13] developed in the context of computer aided maxillo-facial surgery. To represent the face three anatomical layers [18] namely: epidermis, dermis and hypodermis (from the external topmost layer to internal one respectively) the FE mesh is defined by three discrete layers. The external layer corresponds to epidermis and dermis parts and the next two internal layers model the hypodermis that will include facial musculature. The current version of the mesh is composed of 6344 brick elements (full and degenerated hexahedral elements: SOLID185) (Figure 1). The dimensions of the mesh in directions perpendicular to sagittal, transverse and coronal planes respectively are (table. 1):

Table 1- Bounding size of mesh.

Direction	Medial-Lateral	Posterior-Anterior	Superior-Inferior
Dimension in mm	143.52	127.77	137.81

The outer and inner surfaces of the mesh have been extracted from CT data. Then the volume delimited by these two surfaces has been manually meshed with 8 nodes brick elements leading to a total 8736 nodes forming 6030 hexahedron and 314 wedges. In order to reduce the number of DOF during simulation the mesh was assumed as symmetrical along the sagittal plane which seems reasonable in the context of speech production.

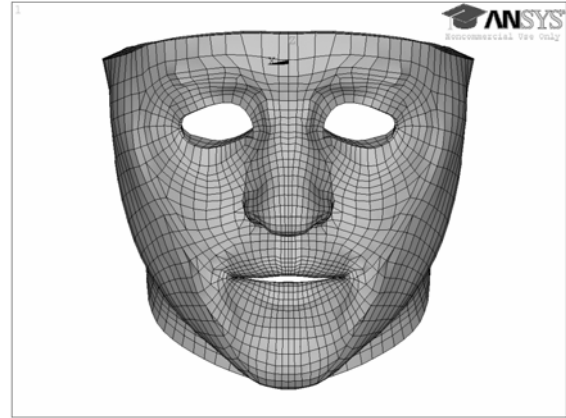


Figure 1- Main Mesh

Element material properties are assumed to follow a hyperelastic model [19]. A simplified 5-parameter Mooney-Rivlin hyperelastic law is used. This model assumes a strain-energy function, W , which its derivative with respect to strain gives stress ($S_{ij}=2\partial W/\partial C_{ij}$, S_{ij} being components of the second Piola-Kirchhoff stress tensor and C_{ij} the components of the right Cauchy-Green deformation tensor) defined by the following expression:

$$W=c_{10}(I_1-3)+c_{01}(I_2-3)+c_{20}(I_1-3)^2+c_{11}(I_1-3)(I_2-3)+c_{02}(I_2-3)^2+((J-1)^2/d) \quad (1)$$

where I_1 and I_2 are respectively the first and second invariants of the right Cauchy-Green strain tensor and J is the determinant of the elastic deformation gradient. In the simplified model only two constants, c_{10} and c_{20} , are different from zero while $d=(1-2\nu)/(c_{10}+c_{01})$ where ν is Poisson's ratio. According to [20]: $c_{10}\approx E/6$ where E is the Young's modulus. The two coefficients c_{10} and d have been calculated from the data reported in [21] with the assumption of mechanical linearity and incompressibility of muscle namely $E=15$ kPa and $\nu=0.499$. The c_{20} coefficient has been determined according to [22]. The computed constants are shown in table 2.

Table 2- Constants of simplified 5-parameter Mooney-Rivlin model for passive tissues.

c_{10} (MPa)	c_{20} (MPa)	d (1/MPa)
2.5e-3	1.175e-3	0.8

The mechanical properties of part of this mesh change with muscle activation to model the stress stiffening effect. More details will be given in the method section.

2.2 Cable Elements: modelling the muscle active part

For modelling muscle activation 3D cable elements (LINK10) are used. These elements are implemented on

top of the facial mesh and model the main directions of muscle fibres. These fibre directions have been extracted from CT data (for the bony insertions and the localization of typical anatomical landmarks) with the help of anatomical facts. The number of fibres per muscle depends on the extent and size of that muscle. Ten orofacial muscles are modelled. The muscle names [18] and the corresponding number of fibres for half of face are shown in Figure 2 and Table 3. These fibres are modelled as a set of contiguous cable elements. Since each cable element is a line in space, the number of cable elements per fibre increases, as a function of the muscle fibre curvature to model it smoothly.

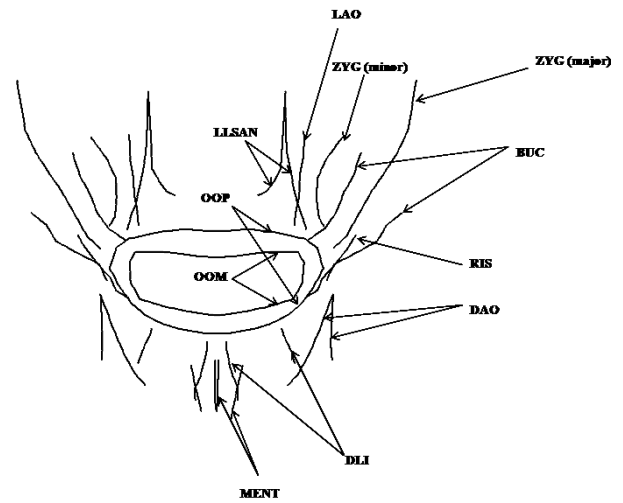


Figure 2- Fibres corresponding to 10 muscles.

Table 3- Orofacial Muscles for half of face

Muscle Name	Abbreviation	Number of Fibres	Total Number of Cable Elements
Levator Labii Superioris Alaeque Nasi	LLSAN	2	12
Levator Anguli Oris	LAO	1	9
Zygomaticus (major and minor)	ZYG	2	15
Risorius	RIS	1	6
Buccinator	BUC	2	12
Depressor Anguli Oris	DAO	2	12
Depressor Labii Inferioris	DLI	2	11
Mentalis	MENT	2	11
Orbicularis Oris Peripheralis (Inferioris and Superioris)	OOP	2	14
Orbicularis Oris Marginalis (Inferioris and Superioris)	OOM	2	14

These cable elements act in tension only and will become slack under compression. These properties are consistent with those of a muscle in the fibre direction.

2.3 Contact Elements

In the model there are two groups of contact elements. The first group is used to couple cable elements with main mesh. The second group is used for modelling the real contact surfaces (lip/lip and lips/teeth).

2.3.1 Coupling Elements

The cable elements are defined independent of the elements of the main mesh, but they are linked to them thanks to *point to surface* contact elements. The *points* (pilot nodes) are extremities of cable elements and the corresponding surfaces of the brick elements which centroid is the closest to cable element extremities. In Figure 3 the cable elements and the corresponding coupling elements for the OOP and ZYG major are shown.

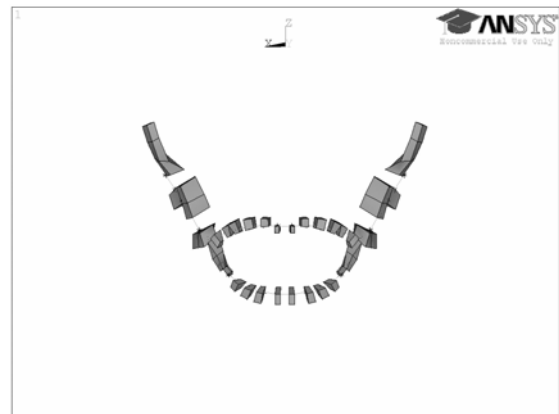


Figure 3- Coupling elements for the OOP and ZYG major.

2.3.2 Contact Surfaces

For modelling lip/lip and lips/teeth contacts, ANSYS contact elements are used. These elements are of surface to surface type (CONTA173 and TARGE170) (Figure 4).

The teeth surfaces on mandible and maxilla have been approximated with a spline surface (Figure 4B) and discretized with quadrilateral rigid target elements. The contact elements have no initial interpenetration and are of sliding type without friction (MU=0).

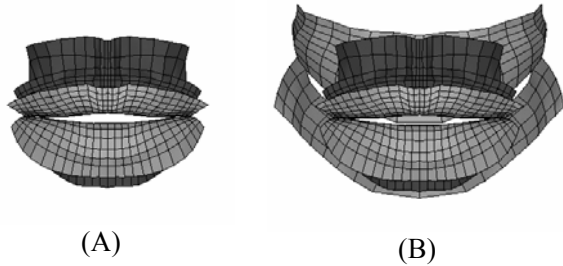


Figure 4- (A) lip/lip and (B) lips/teeth contact elements.

2.3.3 Boundary Conditions

The nodes of the internal layer of the main mesh corresponding to face tissue attachments to the skull are fixed. This no-displacement boundary condition is also applied to the ends of cable elements corresponding to muscle insertions on skull and teeth surface.

3. Method and Theory

3.1 Muscle activation and tissues properties

Muscles behave like a transversely isotropic material with isotropicity in the plane orthogonal to the muscle fibre directions. This means that mechanical properties in the direction of muscle fibres are different from the ones in the cross-fibre direction. Due to force generation in the direction of the muscle fibres and to the fibres tensile characteristics, the transversal bending stiffness increases while the tensile force increases (similar to the stress stiffening phenomenon in cable members or membranes).

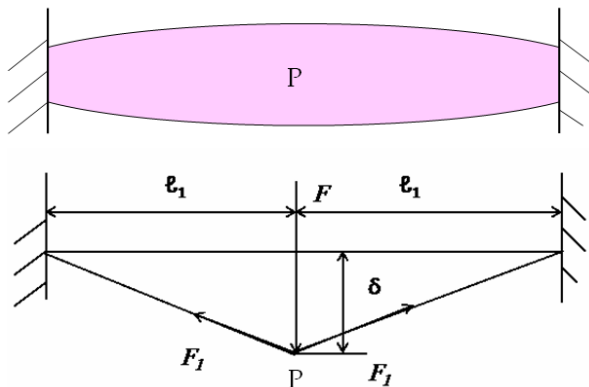


Figure 5- A point P inside a muscle (upper panel) is virtually displaced under the action of a transversal force F that is in equilibrium with fibre forces F_l (upper panel).

This is illustrated in Figure 5 with a simple example of a virtual point P inside a muscle fibre originally at equilibrium under constant muscle activation (force F_l) and then displaced (by δ) because of the action of a force F applied in the muscle transversal direction. Once the new equilibrium is reached (Figure 5 lower panel), assuming a linear relationship between force and displacement, we have:

$$F = 2F_l \frac{\delta}{\ell_1} \left(\frac{1}{\sqrt{1 + \left(\frac{\delta}{\ell_1}\right)^2}} \right) \quad (2)$$

This means that, when δ is negligible as compared to ℓ_1 the muscle transversal stiffness $dF/d\delta$ is proportional to muscle force F_l .

When a muscle is activated, its fibres generate forces that resist to elongation, according to a certain tension-length relation (see for example [1]), and in

a way that increases when activation increases (see for example [23]). In real muscle the fibres

distribution is so dense, that the resistance to elongation of the whole muscle body increases with elongation in the fibres direction. In our model, muscle fibres are not represented in all their details.

They are modelled by a limited number of *localized* macrofibres (typically from one to three). When the muscle is activated, each of these macrofibres generates a force and resists to the elongation, but since the fibres are localized, this resistance does not

apply to the whole body of the muscle. This would not be a realistic behaviour. In our model, in order to compensate for this drawback, the stiffness of the muscle tissues (determined by the mesh elements surrounding the fibres, according to a

neighbourhood algorithm that will be presented below) increases with muscle activation in the fibres direction. Hence, muscle activation is associated both

with a resistance to stress in the direction orthogonal to the fibre direction (the stress stiffening effect) and with a resistance to elongation in the fibre direction. Consequently, it is modelled by an isotropic increase of the young modulus, implemented by modifying the

parameters of the passive constitutive law. This modelling is functionally correct, except for the resistance to compression in the fibres direction. Indeed, it is known that this resistance to compression varies with the

compression rate and is close to zero when this rate is low ([24]). Further improvements will be provided along this line in future works.

3.2 Implementation of muscle activation and stress stiffening

The cable elements generate active muscle force. In the current state of the model, the muscle generation mechanisms are oversimplified. It does not take into account feedback information about length and (or) velocity, but varies as a consequence of a unique central command corresponding to a step function in each time step. For activating a muscle a virtual temperature is used. With decreasing temperature the cable length starts decreasing and therefore each cable exerts force on the main mesh through the coupling elements. With a temperature difference ΔT the force exerted by a cable element will be:

$$F=AE(\varepsilon-\alpha\Delta T) \quad (3)$$

in which A is the cable cross sectional area, E is the Young's modulus and α is thermal coefficient of expansion of the cable elements. Consequently, changing T while keeping the material parameters constant at an arbitrary set of values, will induce changes of the cable force. The material parameters can be used as scaling parameters to boost the level of force at each step.

The variation of the constitutive law associated with muscle activation applies to the mesh elements that are in a close neighbourhood of the muscle fibres. This neighbourhood is determined by an algorithm the considers a sphere (with a radius of the order of the one of the muscle cross sectional dimension) running along the cable elements lines. Each element of the main mesh that intersects the sphere is then determined as a muscle element (see for example Figure 6 for the ZYG and OOP muscles neighbourhoods).

With increase of muscle activation the material properties of these elements will change as a function of parameter T by functionally scaling the factors of the passive hyperelastic law (Figure 7).

3.3 Simulations

Different muscle activation patterns have been used and their influences on facial gestures and mimics have been evaluated. Both static and transient analyses have been performed. In addition to the static analysis that takes into account only the stiffness matrix, full transient analysis takes also into account the effect of inertia and viscosity. In this analysis viscosity is modelled using proportional damping:

$$C=\alpha M+\beta K \quad (4)$$

with coefficients equal to $\alpha=40$ $\beta=0.03$ [25].

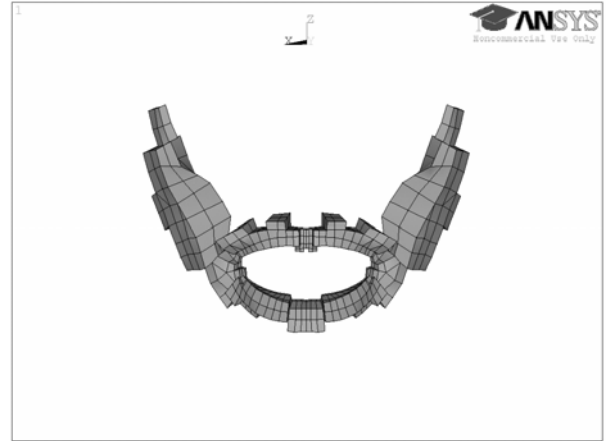


Figure 6- Muscle elements from main mesh corresponding to the ZYG major and the OOP muscles, as selected with the spherical neighbourhood algorithm (see text) with radiuses equal 2 and 3 mm respectively.

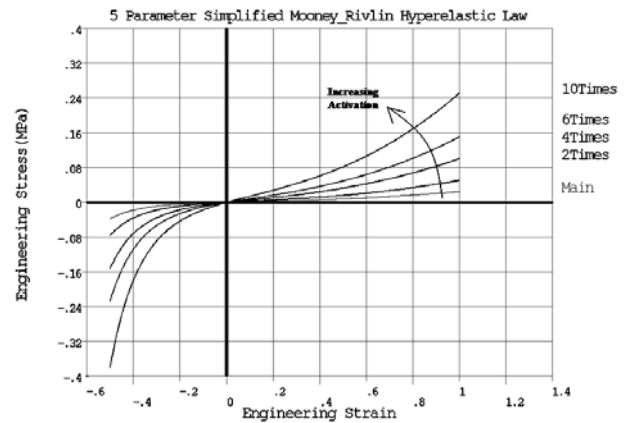


Figure 7- Variation of the constitutive law functionally accounting for stress stiffening effect associated with muscle activation.

4. Results

Figure 8 shows the consequence of the activation of the risorius and Figure 9 shows the impact of activation of the buccinator. In Figure 10 the mimic associated with the coordinated action of OOP and BUC is shown. In all these figures qualitatively these actions are consistent with predictions made from anatomical knowledge.

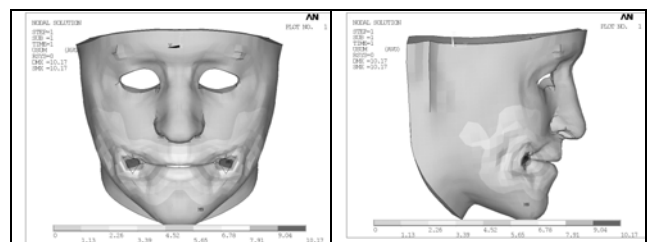


Figure 8- Risorius activation

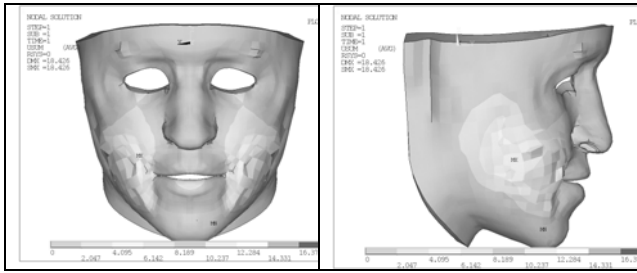


Figure 9- Buccinator activation

The risorius is known to stretch the mouth laterally and to retract the corners of the mouth. This is consistent with the strain depicted in Figure 8

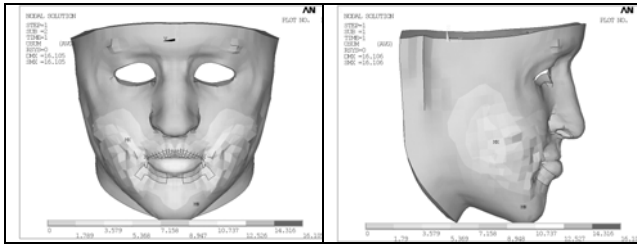


Figure 10- OOP and BUC co-activation

The buccinator has no or little influence on the lips, and essentially act on the cheeks, that are thus compressed against the teeth [26]. Our simulation matches quite well these expectations (Figure 9) the lips have the same shape as in our model at rest, while the strain essentially affects the lower part of the face.

The OOP has been shown in our model to generate a protrusion and a closing of the lips [17], which is consistent with usual hypotheses in the literature, the coordinated action of the buccinators and the OOP generates a closing of the lips. It can be assumed that the stiffening of the cheeks due to the buccinators activation limit the amplitude of the protrusion, which would explain that mainly closure is observed.

For the dynamic analysis full transient analysis is used. The time needed to produce face movements during speech is between 0.1s and 0.3s [27], so we consider 0.1 s as activation time for single muscle activation in transient analysis. Transient analysis of OOP has been used to analyse strain rates. For this purpose maximum strain in each time step is computed and strain rate and average strain rate are calculated (Table 4).

Table 4- Strain rate analysis of OOP activation

Time (s)	Strain	Average Strain Rate (s ⁻¹)	Strain Rate (s ⁻¹)
0	-0.13	-13	0
0.01	-0.13	-6.5	-6
0.02	-0.13	-6.33	-8
0.03	-0.19	-6.75	-6
0.04	-0.27	-6.6	-8
0.05	-0.33	-6.83	-4
0.06	-0.41	-6.43	-6
0.07	-0.45	-6.38	-4
0.08	-0.51	-6.11	-1
0.09	-0.55	-5.6	0
0.1	-0.56		

0	-0.13		0
0.01	-0.13	-13	0
0.02	-0.13	-6.5	-6
0.03	-0.19	-6.33	-8
0.04	-0.27	-6.75	-6
0.05	-0.33	-6.6	-8
0.06	-0.41	--6.83	-4
0.07	-0.45	-6.43	-6
0.08	-0.51	-6.38	-4
0.09	-0.55	-6.11	-1
0.1	-0.56	-5.6	0

Maximum average compressive strain rate in OOP activation is about -6.5 s⁻¹.

Therefore strain rate analysis of muscle activation shows high strain rate in speech movements which justifies the stiffening effect of muscle material properties during movement [24].

5. Discussion and Conclusion

The method used in this paper is simple and enables us dynamic analysis of muscle activation without the need for defining anisotropy which is inherent in muscles. This method simplifies the need for aligning muscle elements along fibre directions which is a difficult task. The three layer defined in the model will help us to define different properties of facial tissues.

References

- [1] T.A. McMahon, *Muscles, Reflexes, and Locomotion*, Princeton, N.J: Princeton University Press, 1984.
- [2] J.D. Humphrey and F.C.P. Yin, "Constitutive relations and finite deformations of passive cardiac tissue II: Stress analysis in the left ventricle," *Circulation Research*, vol. 65, pp. 805-817, 1989.
- [3] J.A. Weiss, B.N. Maker and S. Govindjee, "Finite element implementation of incompressible, transversely isotropic hyperelasticity," *Comput. Methods Appl. Mech. Engrg.*, vol. 135, pp. 107-128, 1996.
- [4] C. A. Yucesoy, B.H.F.J.M. Koopman, P.A. Huijing, and H.J. Grootenboer, "Three-dimensional finite element modeling of skeletal muscle using a two-domain approach:

- linked fibre-matrix mesh model,” *Journal of biomechanics*, vol. 35, pp. 1253-1262, 2002.
- [5] S. Blemker, P.M. Pinsky and S.L. Delp, “A 3D model of muscle reveals the causes of nonuniform strains in the biceps brachii,” *Journal of Biomechanics*, vol. 38, pp. 657–665, 2005.
- [6] A.V. Hill, “The heat of shortening and the dynamic constants of muscle,” *Proc Royal Society, Biological Sciences*, vol. 126, pp. 136-195, 1938.
- [7] F. Zajac, “Muscle and tendon: Properties, models, scaling, and application to biomechanics and motor control,” *Critical Reviews in Biomed. Eng.*, vol. 17, pp. 359–411, 1989.
- [8] V. Ng-Thow-Hing and E. Fiume, “Application-specific muscle representations,” In *Proc. of Gr. Inter.*, W. Sturzlinger and M. McCool, editors., 2002, pp. 107–115.
- [9] J. Teran, E. Sifakis, S. Blemker, V. Ng Thow Hing, C. Lau and R. Fedkiw, “Creating and Simulating Skeletal Muscle from the Visible Human Data Set,” *IEEE TVCG*, vol. 11, pp. 317-328, 2005.
- [10] E. Sifakis, A. Selle, A. Robinson-Mosher and R. Fedkiw, “Simulating Speech with a Physics-Based Facial Muscle Model” In *Eurographics/ ACM SIGGRAPH*, M.P. Cani, and J.O. Brien, editors, Symposium on Computer Animation, 2006.
- [11] Y. Lee, D. Terzopoulos and K. Waters, “Realistic modeling for facial animation,” In *SIGGRAPH’95*, S.G. Mair and R. Cook, eds. New York: ACM Press, 1995, pp. 55–62.
- [12] E. Sifakis, I. Neverov and R. Fedkiw, “Automatic Determination of Facial Muscle Activations from Sparse Motion Capture Marker Data,” *ACM Transactions on Graphics (SIGGRAPH Proceedings)*, TOG 24, pp. 417-425, 2005.
- [13] M. Chabanas, V. Luboz and Y. Payan, “Patient specific finite element model of the face soft tissues for computer-assisted maxillofacial surgery,” *Medical Image Analysis*, vol. 7, pp. 131-151, 2003.
- [14] E. Gladilin, A. Ivanov and V. Roginsky, “A framework for biomechanical simulation of cranio-maxillofacial surgery interventions,” In *Proc of ISMS 2004*, S. Cotin and D. Metaxas, eds., pp. 287-294, 2004.
- [15] J.C. Lucero and K.G. Munhall, “A model of facial biomechanics for speech production,” *J. Acoust. Soc. Am.*, vol. 106, pp. 2834–2842. 1999.
- [16] H. Gomi, J. Nozoe, J. Dang and K. Honda, “A physiologically based model of perioral dynamics for various lip deformations in speech articulation,” In *Speech Production: Models, Phonetic Processes and Techniques*, J. Harrington and M. Tabain, eds., pp 119-134, Psychology Press, 2006.
- [17] M. A. Nazari, Y. Payan, P. Perrier, M. Chabanas & C. Lobos, “A continuous biomechanical model of the face: a study of muscle coordinations for speech lip gestures,” *Proceedings of the eighth International Seminar on Speech Production*, ISSP’08, pp. 321-324, 2008.
- [18] S. Standring, (editor in chief) “Gray’s Anatomy: The Anatomical Basis of Clinical Practice,” 39th Edition, Elsevier Ltd., 2005.
- [19] Y.C. Fung, Y.C., *Biomechanics: Mechanical properties of living tissues*, Springer-Verlag New York Inc, 1993.
- [20] P. Tracqui and J. Ohayon, “Transmission of mechanical stresses within the cytoskeleton of adherent cells: a theoretical analysis based on a multi-component model,” *Acta Biotheoretica*, vol. 52, pp. 323-341, 2004.
- [21] Y. Payan and P. Perrier, “Synthesis of V-V sequences with a 2D biomechanical tongue model controlled by the Equilibrium Point Hypothesis,” *Speech Communication*, vol. 22, pp. 185-205, 1997.
- [22] J.M. Gerarad, J. Ohayon, V. Luboz, P. Perrier, & Y. Payan, “Non-linear elastic properties of the lingual and facial tissues assessed by indentation technique, Application to the biomechanics of speech production,” *Medical Engineering & Physics*, vol. 27, pp. 884-892, 2005.
- [23] R. Wilhelms-Tricarico, “Physiological modeling of speech production: methods for modeling soft-tissue articulators,” *The Journal of the Acoustical Society of America*, vol. 97, pp. 3085–3098, 1995.
- [24] M. V. Loocke, C.G. Lyons and C.K. Symms, “A validated model of passive muscle in compression,” *Journal of Biomechanics*, vol. 39, pp. 2999-3009, 2006.
- [25] S. Buchaillard, P. Perrier and Y. Payan, “A 3D biomechanical vocal tract model to study speech production control: How to take into account the gravity?,” *Proceedings of the 7th International Seminar on Speech Production*, pp. 403-410, 2006.
- [26] P.L. Blanton, N.L. Biggs and R.C. Perkins, “Electromyographic analysis of the buccinator muscle,” *J DENT RES*; 49; 389-394, 1970.
- [27] D. O’Shaughnessy, “A study of French vowel and consonant durations,” *Journal of Phonetics*, vol. 9, pp. 385-406, 1981.